Sensors and Actuators B 224 (2016) 381–390

Contents lists available at ScienceDirect

Sensors and Actuators B: Chemical

journal homepage: www.elsevier.com/locate/snb

Effective organic amine detection by nanoparticle-assembled tin dioxide microspheres: The importance of interparticle porosity on sensing properties

Pan-Pan Jin[a,1], Xiaoxi Huang[b,1], Yong-Cun Zou[a], Li-Jing Zhou[a], Xue Wang[a], Feng Zhang[c], Dejun Wang[d], Guo-Dong Li[a,*]

[a] State Key Laboratory of Inorganic Synthesis and Preparative Chemistry, International Joint Research Laboratory of Nano-Micro Architecture Chemistry, College of Chemistry, Jilin University, 2699 Qianjin Street, Changchun 130012, China
[b] Department of Chemistry and Chemical Biology, Rutgers, The State University of New Jersey, Piscataway, NJ 08854, USA
[c] School of Light Industry and Chemical Engineering, Dalian Polytechnic University, Dalian 116034, China
[d] Department of Chemistry, Tsinghua University, Beijing 100084, China

ARTICLE INFO

Article history:
Received 7 July 2015
Received in revised form 12 October 2015
Accepted 17 October 2015
Available online 20 October 2015

Keywords:
Gas sensor
Oxide
Porous material
SnO_2 microspheres
Amine detection

ABSTRACT

Organic amines are a kind of industrially important starting material for the manufacture of dyes and pharmaceuticals. But monitoring low-concentration amine vapors, especially those with a high molecular weight, is still a challenging task during industrial processes because the low permeability and diffusivity of amines largely limit their interaction with the surface of sensing element. Herein, we report the template-free solvothermal synthesis of uniform nanoparticle-assembled SnO_2 microspheres with an rich interparticle porosity, and the thermal-driven tuning of their porosity structure with the sphere-like morphological preservation. This further allows us to fabricate a sensing film with a tunable interparticle porosity structure and an optimized gas diffusivity in the sensing film. As a result, the optimized SnO_2 sensing film is shown to have the ability to effectively detect low-concentration amine vapors with short response time and high response value in the testing range from 1 to 200 ppm.

1. Introduction

Organic amines, classified as a family of organic compounds containing at least one basic nitrogen atom with unbonded lone pair electrons, are very important intermediates in organic synthesis because of their high reactivity. These compounds are essential in chemical and pharmaceutical engineering to make functional polymers, fertilizers, colorful dyes and drugs [1]. However, most of the organic amines are hazardous to human and can result in severe health problems such as headaches, skin burns, eye irritation, respiratory disease [2]. Furthermore, some amines, like triethylamine, are inflammable and explosive gases. Hence, the concentration of them in the working environment should be controlled properly with the help of some reliable sensors to ensure a safe working environment. In addition, the toxic biogenic amines, such as histamine and tyramine, are generated via the decarboxylation of amino acids during the decay of food due to the relatively higher temperature or enzyme conversion [3–6], especially the protein-rich seafood. Having such unfresh food could cause severe food poisoning. Therefore, researchers have established plenty of methodologies to detect organic amines and the methods are summarized here: the first one is to use chromatography instruments such as high-performance liquid chromatography, gas chromatography [7], to separate and detect organic amines. Another technique is to utilize UV–vis or fluorescence spectroscopy for determination of organic amine by making specific reagents that exhibit some different spectrums, namely peak wavelength and/or intensity, when exposing to amines. These kind of reagents include but not limited to aromatic small molecules [4,8,9], conjugated polymers [10–12], porous metal organic framework [13], ZnO fluorescent film [14], etc. The third approach involves oxide semiconductors to serve as chemiresistors, which show different conductivities upon interacting with the analyte gas. These electrical sensing semiconductor materials include single metal oxide WO_3 [15], MoO_3 microrods [16,17], or mixed metal oxide materials: chromium doped WO_3 [18], SnO_2–ZnO nanocomposite [19], ZnO–Cr_2O_3 heterostructure [20], Cr_2O_3 decorated SnO_2 nanowires [21], thorium incorporated

* Corresponding author.
E-mail address: lgd@jlu.edu.cn (G.-D. Li).
[1] The authors contributed equally to this work.

http://dx.doi.org/10.1016/j.snb.2015.10.063
0925-4005/

SnO_2 [22], ZnO–NiO hetero-nanostructure [2,23]. Except the inorganic semiconductors, organic nanofiber has also been employed as electrical organic amine sensor [24]. Among the aforementioned techniques and materials required for amine detection, oxide semiconductor based chemiresistors have attracted extensive attention due to their tremendous advantages: no expensive and complicated instruments are required; the semiconductors are stable and can be made into a portable device with very low power consumption and small size; the most important point is that they show excellent gas sensing properties.

As we mentioned above, the chemiresistors can give different signals when the amines interact with their surface, so the synthesis of high surface area materials with appropriate pore size is necessary and plays important roles not only in gas sensing fields, but also other applications. This stimulates the exploration of various synthetic approaches to prepare different kinds of such nanomaterials. Herein, we focus on tin dioxide, an important n-type wide-band gap (3.6 eV at 300 K) semiconductor, to constitute porous amine sensing material. SnO_2 has been prepared by many methods which can be summarized as three general ways: the first one is hard template synthesis, during which hexagonal mesoporous silica SBA-15 [25–27], cubic KIT-6 [26], or polymer templates [29,30] were used as sacrificial material to generate porous SnO_2; the second method is soft template synthesis, in which polyvinyl pyrrolidone [31], oleic acid [32], sodium dodecylsulfate and hexadecyl-2-pyridinylmethylamine [33], cetyl trimethylammonium bromide [34], or sodium alginate [35] were employed as pore filling agents to form porous SnO_2 after removal of these templates; the last approach is the template free synthesis of SnO_2 which does not need surfactant or hard template to create the pores [36–40].

In this work, we have successfully synthesized uniform nanoparticle-assembled SnO_2 microspheres with a highly porous structure via a template-free route different from aforementioned methods, and the formation mechanism of such porous materials is discussed. The surface area, pore size, nanoparticle size can be tuned via the thermal treatment of the resulting SnO_2 microspheres. After annealing treatment, the materials show excellent sensing performance toward organic amine and the relationship between the sensing properties and interparticle pore structures are discussed as well.

2. Experimental

2.1. Chemicals and reagents

Stannic chloride pentahydrate ($SnCl_4{\cdot}5H_2O$) was purchased from Tianjin Fuchen Chemical Reagent Factory. Glycerol was purchased from Sinopharm Chemical Reagent Co. Ltd. Ethanol and isopropanol were purchased from Beijing Chemical Factory. Triethylamine with a purity of >99% and a water amount of ~0.2% was purchased from Sinopharm Chemical Reagent Co., Ltd. All the above chemicals were used without further purification. Deionized water was used through the experiments.

2.2. Synthesis of porous SnO_2 microspheres

In a typical synthesis, $SnCl_4{\cdot}5H_2O$ (0.35 g, 1 mmol) was dispersed in a mixed solution containing glycerol (8 mL) and isopropanol (30 mL). The resulting mixture was transferred into a 60 mL Teflon-Lined autoclave, followed by thermal treatment at 180 °C for 12 h. After cooling to room temperature, the resulting precipitate was centrifuged and washed thoroughly with ethanol several times, then dried in an oven overnight at 80 °C in air to afford porous SnO_2 microspheres. In order to study the effects of porosity structure on SnO_2 materials' sensing performance, five more samples were prepared by heating the as-synthesized SnO_2 microspheres in air at 450, 550, 650, 750, or 850 °C for 2 h with a ramping rate of 2 °C/min.

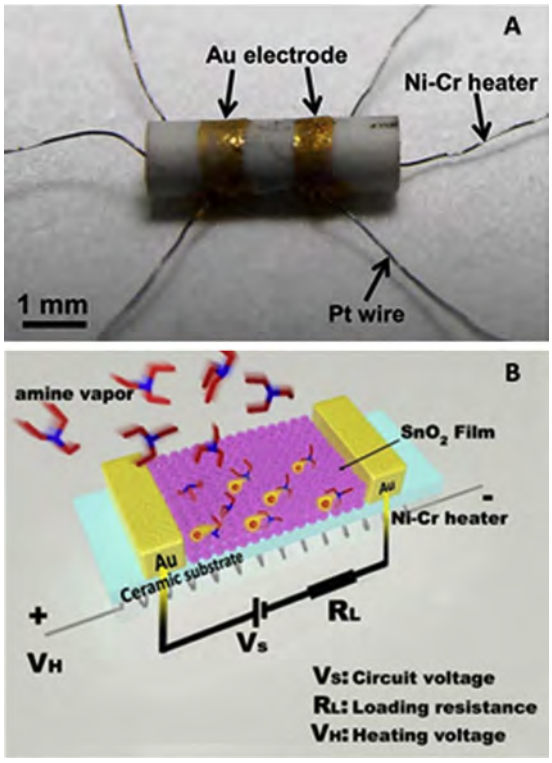

Scheme 1. (A) Digital image of the sensor composed of different parts: ceramic tube, two Au electrode, four Pt wires and a Ni-Cr wire. (B) Schematic illustration of the electric circuit for the sensing of amine vapor.

2.3. Material characterizations

The powder X-ray diffraction (XRD) patterns were performed with a Rigaku D/Max 2550 X-ray diffractometer using Cu Kα radiation (λ = 1.5418 Å) operated at 200 mA and 50 kV. The scanning electron microscopic (SEM) images were carried out on a JEOL JSM 6700F electron microscope. The transmission electron microscopy (TEM) and high-resolution TEM (HRTEM) images were obtained on a Philips-FEI Tecnai G2S-Twin. The infrared (IR) spectra were recorded on a Bruker IFS 66V/S FTIR spectrometer using KBr pellets. The thermal gravimetric analysis curve was recorded on a NETZSCH STA 449C TG thermal analyzer from 25 to 800 °C at a heating rate of 10 °C min^{-1} in air. BET surface area and BJH pore diameter were measured by using a Micromeritics ASAP 2020M system.

2.4. Sensor fabrication and testing

In order to assemble the gas sensor, viscous slurry of the obtained sample was put into a ceramic tube with a diameter of 1 mm and a length of 4 mm. As shown in Scheme 1, the ceramic tube was constructed with a pair of gold electrodes and four platinum wires on two sides of the tube. The operation temperature of the sensor was controlled by the nickel-chromium heating wire located in the center of the tube. To ensure proper comparison between different materials, the same method was used to prepare the sensors, with the only difference being the SnO_2 materials in the tube. A commercial CGS-8 Gas Sensing Measurement System (Beijing Elite Tech Company Limited) was employed to conduct all the gas sensing evaluation.

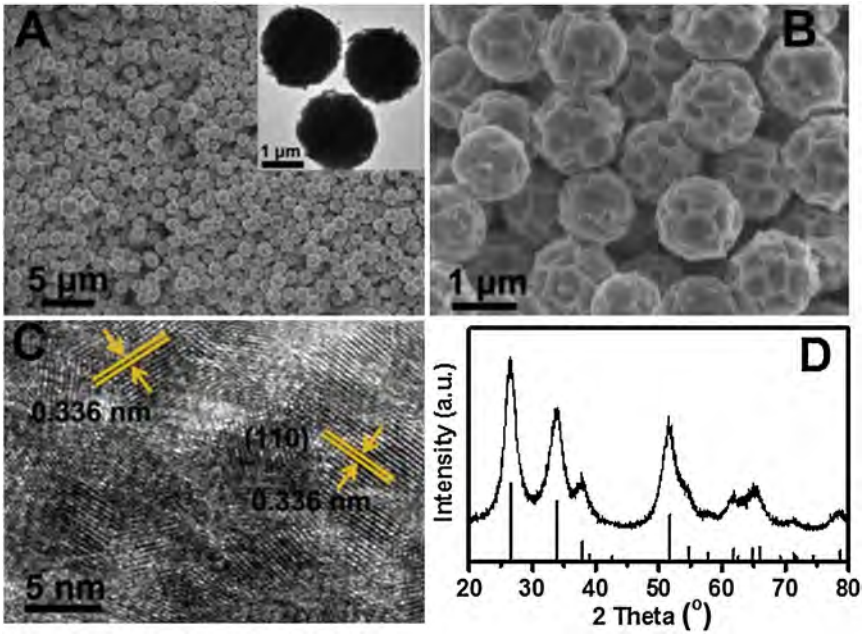

Fig. 1. (A) Low and (B) high magnification SEM images of as-synthesized SnO_2 obtained after solvothermal reaction. (C) High resolution TEM image of the SnO_2 nanocrystals which constructed the microspheres. (D) XRD patterns of the as-synthesized SnO_2 sample. The inset of (A) shows the TEM image of the as-synthesized SnO_2 microspheres.

Gas sensing properties were evaluated using a static test system which included a 1 L test chamber. In order to prepare the sample gases, a certain amount of the liquid sample (e.g., triethylamine) was transferred into the test chamber using a microsyringe and maintained for >60 min to give a homogenous atmosphere. In fact, environmental air with a relative humidity of ~40% was used as a diluting gas to obtain the desired concentration of target gases during the preparation of the sample gases. Note that the humidity (~40%) of the environmental air and the sample gases was measured by a humidometer, and the result showed that there is no humidity difference between the base air and the sample gases. For measurement, the sensor was put into the test chamber to get a stable reading of resistance R_g. To recover the sensor after the R_g was stable, the sensor was exposed to fresh air. The resistance of sensor in environmental air with a relative humidity of ca. 40% was tested as R_a. Finally, the response was calculated as R_a/R_g. The response time is defined as the time required for the resistance to become $[R_a - 90\%(R_a - R_g)]$ upon interacting with the target gas, similarly, the recovery time is defined as the time need to allow the resistance to become $[R_g + 90\%(R_a - R_g)]$ after put in the fresh air. 180 °C was selected as the optimal operation temperature in our sensing measurements.

3. Results and discussion

As illustrated in Scheme 2, the as-synthesized porous SnO_2 microspheres were prepared via a simple one step solvothermal treatment of $SnCl_4{\cdot}5H_2O$ in glycerol and isopropanol. The obtained material was fully characterized by various techniques including SEM, TEM, XRD, BET, TGA and FTIR to study its morphology, structure and composition. The obtained microspheres have a uniform particle size of 1.5 μm as shown in the SEM images and TEM image (Fig. 1A) and the surface of these particles display wrinkled structures (Fig. 1B) due to the growth of nanoplate-like SnO_2 on the surface, which is helpful to achieve higher surface area and larger pores. The thickness of these nanoplates on the microspheres' surface are about 100 nm, and this kind of structure is not observed in the SnO_2 prepared by other methods [25–40]. A closer observation via the high resolution TEM image indicates that the microspheres

Scheme 2. Preparation of the as-synthesized porous SnO_2 via solvothermal treatment.

are assembled by a lot of tiny individual nanocrystals with an average diameter of ca. 5 nm (Fig. 1C). The distance between the parallel lattice fringes are determined to be 0.336 nm, corresponding to the distance of (1 1 0) planes, in agreement with previous reports for SnO_2 [36,38]. In addition, all of the peaks in XRD patterns (Fig. 1D) can be indexed to tetragonal rutile SnO_2 phase without other unrelated signal, confirming that the obtained product is SnO_2. The nitrogen adsorption–desorption isotherms of the as synthesized SnO_2 microspheres show a similar type-IV isotherm with an obvious hysteresis loop (Fig. 2) [40], indicating that the SnO_2 materials are highly porous, which is further confirmed by the BJH pore size distribution with pore diameter ranging from ca. 1 nm to 20 nm with a peak pore size at 1.7 nm. The resulting BET surface area for this sample is as high as 204 $m^2\ g^{-1}$. This is expected because the as-synthesized SnO_2 are constructed by many nonporous small nanocrystals, and the micropores/mesopores are easily formed between the adjacent nanocrystals. Therefore, the as-synthesized SnO_2 microsphere is porous.

Besides the highly porous SnO_2 microspheres prepared from the procedures we mentioned above, another two routes were attempted at the same time to elucidate the formation mechanism of such a porous structure. The first one is solvothermal treatment of $SnCl_4{\cdot}5H_2O$ in isopropanol without any glycerol, leading to

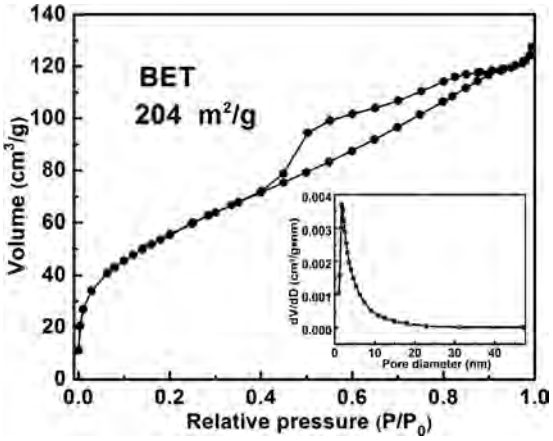

Fig. 2. Nitrogen adsorption–desorption isotherms of as-synthesized SnO_2 microsphere. The inset shows the BJH pore size distribution curve.

the material of less porous SnO_2 (denoted as SnO_2-IPA) nanoparticles. The SnO_2-IPA has smaller particle size of ca. 100–400 nm compared with the as-synthesized SnO_2 as seen from the electron microscope images (Fig. S1). Similarly, SnO_2-IPA nanoparticles are constructed by small crystals about 5 nm as shown in the high resolution TEM image (Fig. S1D). However, it should be noted that no wrinkled surface morphology is observed in this sample from the high magnification SEM image (Fig. S1B). The nitrogen adsorption–desorption isotherms was applied to further study the pore structure of SnO_2-IPA, displaying a lower surface area of 150 $m^2\,g^{-1}$. The corresponding BJH pore size distribution curve shifts to smaller pore diameter region (Fig. S2), indicating that the small SnO_2 crystals are packed more closely with each other in SnO_2-IPA and thus lead to reduced surface area and pore size. On the contrary, another control experiment is the reaction of just $SnCl_4{\cdot}5H_2O$ with glycerol, giving no products. These results suggest that isopropanol is crucial for the formation of SnO_2, while the glycerol is responsible for the assembling of tiny nanocrystals into a highly porous structure. This may be attributed to the inter molecular hydrogen bonding generated by the glycerol as well as its chelating ability, which can assist the separation of SnO_2 nanocrystals and make them pack less closely with each other to create a higher surface area and larger pore size.

There are some unsaturated bonds on the surface of nanocrystals, which help to interact with water molecules under ambient condition, and this has been proved by experiments and simulation [42,43]. Thermal gravimetric analysis (TGA) result was obtained by heating the sample from room temperature to 800 °C in air to ensure the decomposition of all the organic components. As seen from the TGA trace (Fig. 3A), two obvious weight loss stages were observed. The first one, from 25 °C to 100 °C, showed about 6.4% weight loss, representing the release of water or solvent adsorbed on the surface. With the temperature continuously increasing, until 450 °C, the second stage appeared with a decrease of 26.2 wt%, due to the large amount of organic compound located on the surface. Aside from the above two apparent stages, the samples' mass gradually reduced from 450 °C to 800 °C, because of the elimination of surface OH groups on SnO_2 nanocrystals, which cause the growth of smaller nanocrystals into bigger ones. The desorption of O^- and O^{2-} from the SnO_2 may also lead to the weight loss at high temperature [42,44]. The FTIR spectrum (Fig. 3B) revealed some significant bands, the peaks at 2925, 2880 cm^{-1} are related with C—H bond, the peaks at 3425, 1630 cm^{-1} are attributed to the stretching vibration of OH groups and bending vibration of the adsorbed water molecules, respectively, confirming the presence of organic compound and water in the SnO_2 material, which is

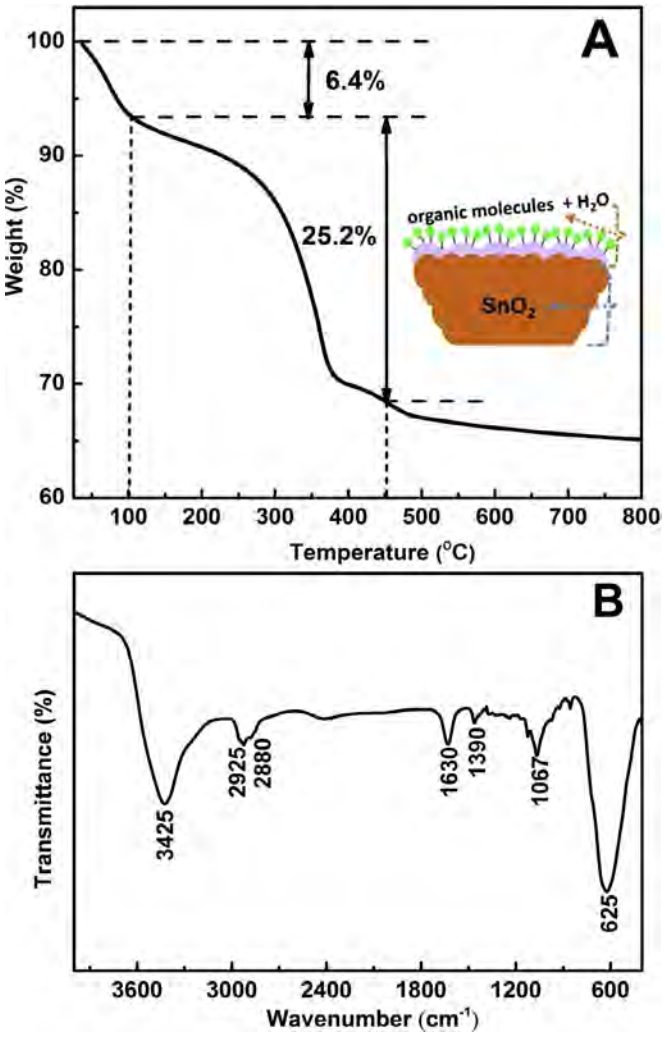

Fig. 3. TGA and FTIR of the as-synthesized SnO_2 sample.

consistent with the TGA results. The signal at around 625 cm^{-1} is related with the Sn—O lattice vibration [44]. Both TGA and FTIR confirm the presence of large amount of water and organic compounds on the surface of as-synthesized SnO_2, indicating that these molecules may have participated into the nanoparticles' growth and assembling, and this is why such a porous structure would be achieved. However, as we know, the gas to be detected, like organic amine, should interact with the surface of SnO_2 to stimulate some resistance alteration and that is how most semiconductors detect the gas molecules. Thus, the existence of such large amount of water and organic compounds on the SnO_2 surface could greatly restrict the interaction with the organic amine to be measured. Consequently, the obtained as-synthesized SnO_2 were annealed in air at different temperatures ranging from 450 °C to 850 °C to remove the surface adsorbed compounds and investigate the correlation between gas sensing properties and structures characteristics of SnO_2 at different temperatures. These samples are denoted as S450, S550, S650, S750, S850, respectively, where the number represent the pyrolysis temperature.

Electron microscopy was further employed to study the morphologies of the annealed samples. The low magnification SEM images (Fig. 4) for the annealed SnO_2 demonstrate very similar spherical morphology with alike particle size inherited from the as-synthesized SnO_2. It should be noted that the annealing does not lead to coagulated particle, uniform microspheres are observed in all low magnification SEM images. In addition, it is seen that

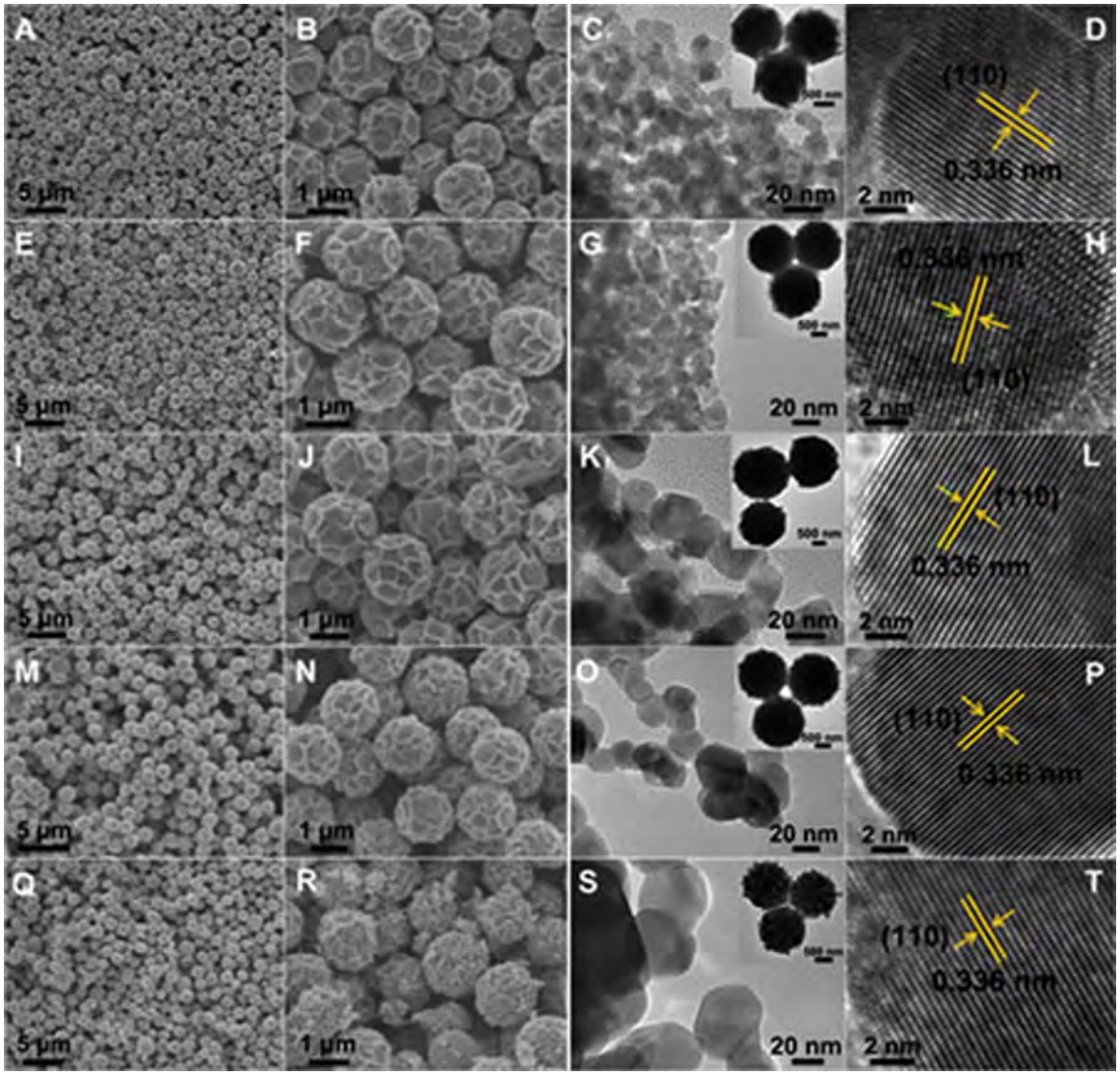

Fig. 4. Low and high magnification SEM images and high resolution TEM images of S450 (A–D), S550 (E–H), S650 (I–L), S750 (M–P), S850 (Q–T).

the surface wrinkled morphology for the samples obtained from 450 °C to 750 °C maintained, with a thickness of ca. 100 nm, while this kind of structure was destructed at the very high temperature of 850 °C. On the other hand, the sizes of the single small crystals gradually increase with the increasing temperature. All of the samples show clear (1 1 0) face with a distance of 0.336 nm, same with the as-synthesized SnO_2. The type IV nitrogen adsorption/desorption isotherms (Fig. S3) demonstrate clear hysteresis loops [41], indicating that the materials are porous. The total pore volume of all the samples are shown in Table S1. The BET surface area and pore sizes of these samples are summarized in Table 1, showing a decreasing tendency of surface area and an increasing trend of interparticle pore size when the pyrolysis temperature increase. This is because the growth of smaller SnO_2 crystals into larger one when the temperature was rising, and the bigger crystals will result in smaller surface area. The pores are generated via the assembling of SnO_2 crystals, the bigger the crystals are, the larger the pore size will be. Hence, we can have a series of SnO_2 samples with tunable surface areas and pore diameters for the organic amine sensing application. XRD patterns (Fig. 5) of these samples demonstrate Bragg's diffraction peaks for SnO_2, with increasing temperature, the peaks become stronger and sharper, indicating the enhanced crystallinity of SnO_2 and the growth of the nanocrystals.

Table 1
Comparison of the crystal sizes, BET surface areas and pore diameters for samples S450, S550, S650, S750, S850, and the corresponding D_k for TEA gas at 180 °C.

Sample name	Crystal sizes (nm)	BET surface area ($m^2\ g^{-1}$)	Pore diameter (nm)	Pore radius (nm)	$D_k \times 10^{12}$ $nm^2\ s^{-1}$
S450	10	44	15	7.5	1.54
S550	13	25	29	14.5	2.98
S650	18	20	46	23	4.72
S750	23	13	70	35	7.19
S850	32	9	98	49	10.1
S750-IPA	25	12	50	25	5.0
Com-SnO_2	50–800	6	<25	<12.5	<2.5

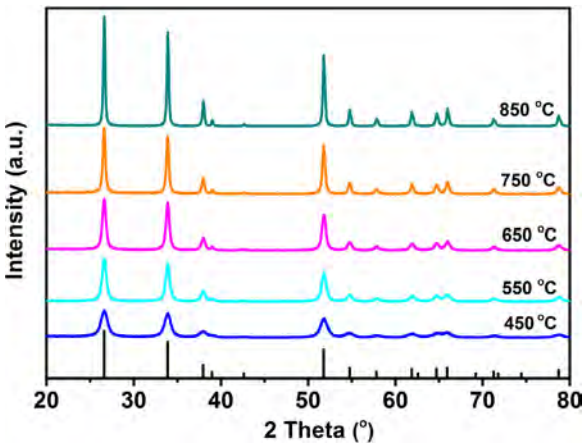

Fig. 5. XRD patterns of S450, S550, S650, S750, S850.

Triethylamine (TEA), an important compound for organic synthesis, was used as a testing gas to evaluate the sensing properties of SnO_2 prepared at different temperatures in our experiment. In order to investigate the relationship between the sensing property and the material's microstructure, the possible effects of relative humidity on the material's sensing properties must be avoid first, because water molecules can directly interact with SnO_2-based sensor, and correspondingly, relative humidity possibly lead to the change of resistance of SnO_2-based sensor. In view of the facts that the resistance of our sensor only varied with a large change in relative humidity (please see Fig. S4) and the humidity (~40%) of the environmental air and the sample gases was kept the almost same in our experiment, our sensor can be used for the detection of triethylamine.

Because the performance of gas response on semiconductor are usually related with the operation temperature, the best operation temperature was selected via comparison of the response (R_a/R_g), response time and recovery time at various temperatures in the presence of 100 ppm TEA using sample S750 as an example. The response–temperature curve (Fig. 6A) indicate that the highest response ($R_a/R_g = 148$) was obtained at 150 °C, and then decrease slightly ($R_a/R_g = 130$) when the temperature decrease to 120 °C, or significantly decrease ($R_a/R_g = 21$) when the temperature increase to 210 °C, after that, the response remain very low, $R_a/R_g \leq 10$, until 330 °C. This kind of inverse V-shaped relevance between the temperature and sensor response is representative for SnO_2-based gas sensors [35,39]. The response time for S750 is very fast, less than 2 s for all the temperatures from 150 °C to 330 °C (Fig. 6B). However, the recovery time became longer when the temperature decreased. Considering all the factors mentioned here, 180 °C was selected as the operation temperature because it has relatively high response ($R_a/R_g = 96$), fast response time (ca. 1 s) and acceptable recovery time (680 s).

Fig. 6C shows the representative dynamic response–recovery curves of S750 in the presence of increasing TEA concentrations (from 1 ppm to 200 ppm) at 180 °C. It is seen that the sensor has a wide response range for TEA gas from 1 to 200 ppm. When the sensor is exposed to 1 ppm TEA gas, its resistance rapidly decreases, and the resistance returns quickly to the original value when the sensor is exposed to air again. Similar response and recovery behaviors are also observed for the detection of TEA gas with a higher concentration, but a higher TEA concentration results in a lower resistance. This result, coupled with the recent studies on the interaction between oxide semiconductor and organic amine [45–47], indicates that the decrease of the sensor resistance might originate from the direct electron transfer from organic amine to SnO_2 semiconductor. However, this possible scenario beg for further in-depth

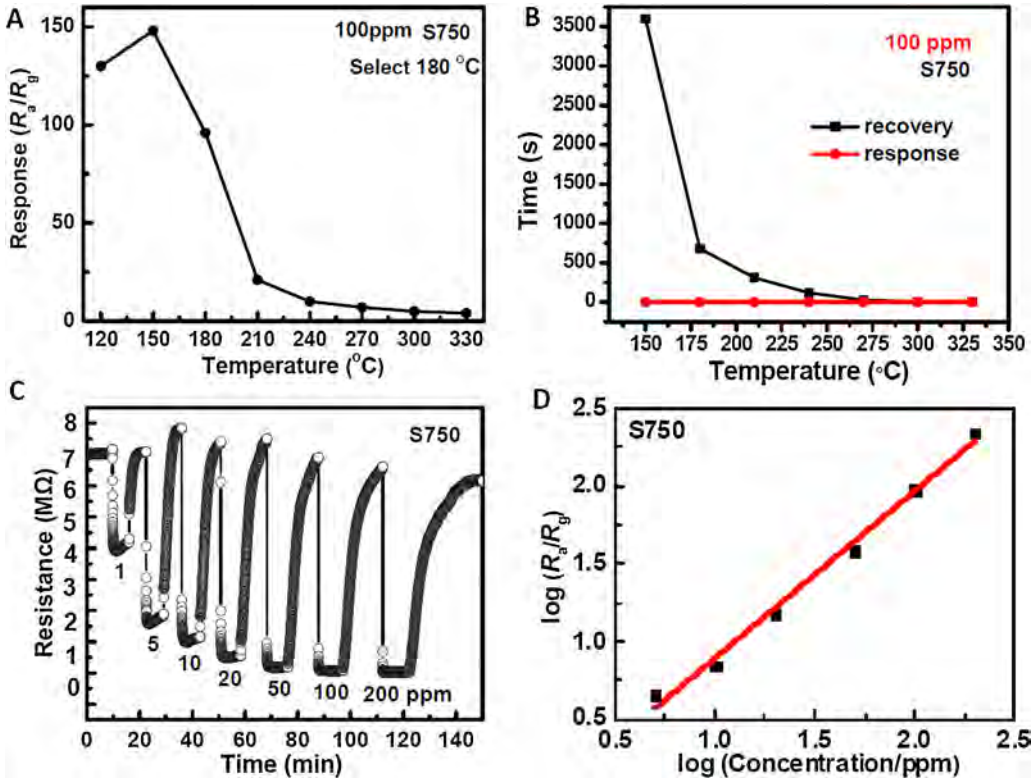

Fig. 6. (A) Response to 100 ppm TEA at different operation temperature for sensor fabricated by S750. (B) Response and recovery time for the determination of 100 ppm TEA using S750 as the sensing material. (C) Dynamic response–recovery curves of the sensor based on S750 at 180 °C. (D) Linear curve between the logarithm of response and logarithm of the concentration for S750.

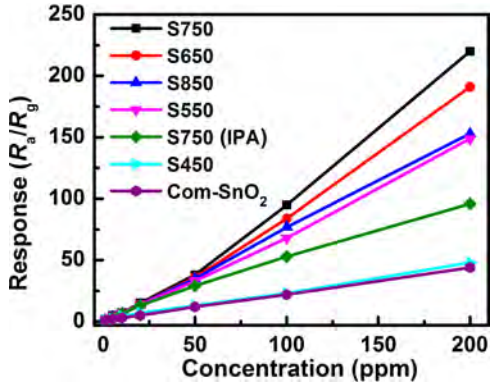

Fig. 7. Response comparison in presence of various concentrations of organic amine for SnO_2 prepared at different temperatures.

mechanistic investigation. Except the qualitative measurement of TEA, the logarithm of the sensor response reveals a very good linear relationship on the logarithm of TEA concentration testing range, with the R^2 equal to 0.99, indicating that it can serve as a good candidate for quantitative analysis of TEA.

In order to investigate the influence of SnO_2 interparticle pore structure on their sensing performance, the detection ability for TEA by S450, S550, S650, S850 based sensors was evaluated at different concentration of TEA atmosphere. As shown in Figure S5, the sensing response gradually increase when the concentration increase, and similar with S750, very good linear fitting curves for logarithm of the response and that of the TEA concentration are obtained in all the samples. Nevertheless, as summarized in Fig. 7, all of these samples display relatively lower response compared with S750 sample. In addition, S750-(IPA), obtained from SnO_2-IPA pyrolyzed at 750 °C, which possess similar surface area (12 m^2/g) but smaller pore size (Fig. S6) compared with S750, and commercial SnO_2 materials were used to test the TEA under the same conditions (Figs. S7 and S8). As compared with the materials annealed at different temperatures from as-synthesized SnO_2 (Fig. 7), S750-(IPA) demonstrates worse response compared with S550, S650, S750, S850, only higher response than S450. It is also worth to mention that almost all of the samples show higher response to TEA at various concentrations compared with commercial SnO_2 material, except S450 exhibit similar response compared with commercial one. These results prove the advantages of our template free synthetic approach for synthesis of porous SnO_2 materials, as well as the importance of glycerol during the preparation. The commercial SnO_2 sample was characterized by nitrogen adsorption/desorption, XRD and SEM techniques (Fig. S9). The primary property of commercial SnO_2 is the relatively small pore size and very small pore volume (Table S1), which might limit its interaction with organic amines.

For the materials annealed from 450 °C to 850 °C using as-synthesized SnO_2 as precursor, it is very interesting that the best response activity was achieved at 750 °C, instead of the sample with the highest surface area. It is reported that square of the sensor response should be linearly increasing with the reciprocal of particles size if the entire surface of the sensing materials can be utilized for the sensor response [48,49]. A plot of square of sensor response to the reciprocal of particle size is shown in Fig. 8A, no linear increasing curve is obtained, indicating that except the surface area, some other factors must also influence the sensing performance. As we know, the target gas has to diffuse into the porous structure of the sensing material to take advantage of its high surface area and the porosity of sensing materials play a very important role in terms of diffusion [50]. The gas diffusion in the pores with radius from 1 or 2 to 100 nm is known to be governed

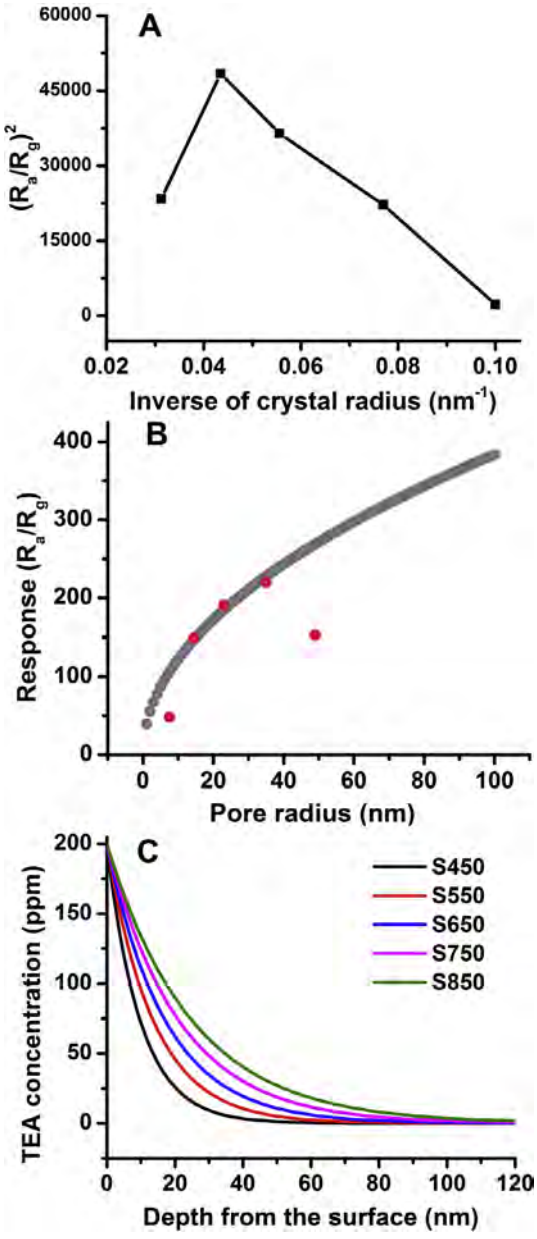

Fig. 8. (A) Relationship between the square of sensor responses to TEA for SnO_2 with different crystal sizes due to the difference in thermal treatment temperature and the inverse of crystal radius. (B) Simulated sensor response to 200 ppm TEA at 180 °C as a functional of materials' pore radius. The red data points are the experimental results with pore radius of 7.5, 14.5, 23, 35, 49 nm, respectively. (C) Simulated curve for concentrations of TEA and the depth from the surface of SnO_2 with different pore sizes. T, L, and k were constant at 180 °C, 750 nm and 1.61×10^{10} s^{-1}. (For interpretation of the references to color in this figure legend, the reader is referred to the web version of the article.)

by the Knudsen diffusion [51]. In Knudsen diffusion mechanism, the diffusion coefficient (D_k) can be calculated from the equation below [51]:

$$D_k = \left(\frac{4r}{3}\right)\left(\frac{2RT}{\pi M}\right)^{1/2} \quad (1)$$

in which r represents the pore radius, R is the gas constant, T is the surrounding temperature and M is the molecular weight of the target gas. Based on this equation, the D_k for TEA in S450, S550, S650, S750, S850 was calculated at the operating temperature of 180 °C and the results are shown in Table 1. With the increasing pore radius, the diffusion coefficient also increases and this helps

the TEA to penetrate deep into the sensing materials, increasing the utilizing factor of the sensing materials, resulting to a better sensor response. However, the response becomes worse when the D_k reach the highest value of 10.1×10^{12} nm^2 s^{-1}, which may because of the decreased surface area, limiting the interaction of target gas and SnO_2. The pore radius could affect the diffusion coefficient of gas, and further change the resulting sensing response. The function between D_k and S can be expressed as Eq. (2) below according to previous theoretical concept [49,51].

$$S = \frac{R_a}{R_g} = 1 + A \times \frac{C_{A,S}}{m} \times \tanh(m), \quad m = L\left(\frac{k}{D_k}\right)^{1/2} \tag{2}$$

Some more parameters are involved in Eq. (2), A is the sensitivity coefficient with a constant value and unit of ppm^{-1}. $C_{A,S}$ represents the concentration of target gas on the surface. L is the film thickness, which could be equivalent to the radius of SnO_2 microspheres as 750 nm in our experiment. k is the rate constant for the reaction between adsorbed oxygen species on SnO_2 and reducing gas. D_k is the diffusion coefficient, which is related with pore size as we mentioned above. By using Eq. (2) and experimental data for S650, S750, an estimated k and A were obtained as 1.61×10^{10} s^{-1} and 40.2 ppm^{-1}, respectively. Then a simulated result was obtained based on Eq. (2) along with the calculated $k = 1.61 \times 10^{10}$ s^{-1}, $A = 40.2$ ppm^{-1}, $L = 750$ nm, as the constant values. The result (Fig. 8B) reveals an increasing tendency between the sensor response and pore radius. Our experimental response for S450, S550, S650, S750, S850 are also shown in the same figure with red color. It clear that response for S550, S650 and S750 are very well consistent with the simulated curve, the response for S450 also follows the trend that smaller pores give lower response, only a little off the curve. The only one S850 displays actual result much away from the curve, could be due to its lower surface area and larger particle size as we mentioned above. In order to further explain the increasing response as a function of the pore radius, the concentrations of target gas inside the sensing materials were simulated as well based on the equation below [49,51]:

$$C_A = C_{A,S} \times \frac{\cosh(m - m \times x/L)}{\cosh(m)}, \quad m = L\left(\frac{k}{D_k}\right)^{1/2} \tag{3}$$

For the simulation, the calculated $k = 1.61 \times 10^{10}$ s^{-1}, and $L = 750$, $T = 180$ °C, $C_{A,S} = 200$ ppm were used, and different D_k (Table 1) for SnO_2 samples annealed at various temperature were used. x value in Eq. (3) represent the depth from the surface. The results demonstrate a significant decrease of gas concentration upon going deep into the sensing materials. Faster decrease tendency is observed for smaller pores, for example, at the depth of 40 nm, the S450 only allow 3.35 ppm TEA to penetrate, while S850 allow 40.4 ppm TEA to penetrate. These results again confirm that larger pores are more effective for TEA to diffuse into and increase the utility percent of all the sensing materials. Moreover, here we can answer more about the decreased response for S850. The sensing films we prepared here contain two types of diffusions, one is the external diffusion utilizing the space between the micro clusters, and another one is the internal diffusion inside the micro cluster involving the pores created by the packed SnO_2 nanocrystals (Scheme 3). For the former one, it is less restricted because the pores assembled via microspheres are very large, so the internal diffusion could govern the sensor performance more significantly. It is seen that the TEA concentrations become negligible until the thickness of the sensing material is ca. 100 nm based on our simulation results. Therefore, the nanoplates formed wrinkled morphology, possessing a thickness of ca. 100 nm (Fig. 4B, F, J, and N), could be an important advantage for the internal diffusion process. However, the wrinkled structure is no longer exiting in S850 (Fig. 4R), that is why it revealed lower response. In addition, pore size not only influence

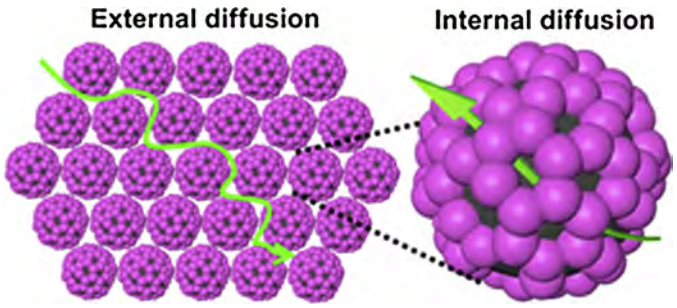

Scheme 3. Schematic representative of the gas diffusion in the sensor prepared by SnO_2 materials synthesized via template-free method.

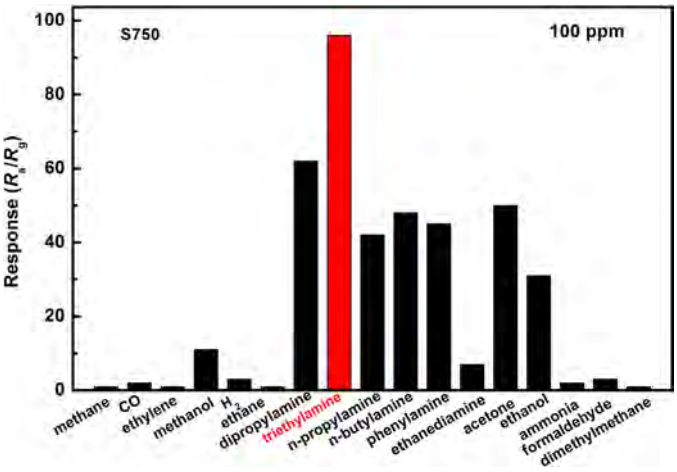

Fig. 9. Selectivity of S750 in the presence of different gases (100 ppm).

the diffusion of target gas, but also increase the electrical resistance because the pores have poor conductivity [48]. The sensor response for SnO_2 are defined as R_a/R_g, in which the increase of R_a or the decrease of R_g can lead to enhanced response. In fact, the increasing pore radius does not lead to very significant increase of electrical resistance when the pore radius less than 23 nm, but after that the resistance increase a lot both in air and in target gas atmosphere (Fig. S10). So the final response will be determined by the one that increase faster, this could be expressed as the slope between two points on the graph. In Fig. S9A, the slope 2 is 2.6 times higher than slope 1, while in Fig. S9B, the slope 2 is 4.8 times higher than slope 1, indicating that the resistance in target gas is increasing much faster than that in air for S850, that is why the ratio of R_a/R_g decrease for S850. Based on above discussion, it is concluded that an optimization of pore size should be conducted for the sensing material to show the best performance.

We further studied the selectivity of S750 in the presence of 100 ppm different gases at the same operation temperature of 180 °C. As shown in Fig. 9, S750 can give significant response for all kinds of nitrogen containing compounds, except the ethanediamine and ammonia. In terms of primary amine (n-propylamine, $R = 42$), secondary amine (dipropylamine, $R = 62$) and tertiary amine (TEA, $R = 96$), the response increase when more alkyl groups are connected with nitrogen, probably due to the increased electron donation effect of alkyl groups. The lower response for ethanediamine ($R = 7$) could probably be attributed to the heavily intramolecular and/or intermolecular hydrogen bonding, which limit the interaction between the nitrogen and sensing materials. Except the organic amines, S750 can also detect oxygen containing compounds, such as acetone, ethanol, and methanol. The responses for hydrocarbon (methane, ethylene, ethane, dimethylmethyane) and other gases (CO, H_2, formaldehyde) are very low. The most

important point is that S750 shows highest response value for 100 ppm of TEA, indicating that it could be a good material for selective TEA sensing application.

4. Conclusions

In summary, uniform nanoparticle-assembled SnO_2 were prepared successfully by a template-free route and glycerol was found to be significant for the formation of highly porous material. Thermal treatment of the as-synthesized SnO_2 at different temperatures gave a series of materials with various surface areas, pore size and nanoparticle size; and the surface adsorbed organic compounds and water were removed at the same time. The TEA was used as the target gas to evaluate the sensing properties of the annealed samples, moreover, theoretical model was applied to study the gas diffusion as well as the relevance with their sensing properties. The SnO_2 materials we prepared were proved to be an effective candidate for organic amine sensing. In addition, the template free method also have potential to prepare other porous inorganic materials for many other applications.

Acknowledgments

This work was supported by the NSFC (21371070, 21401066, 21401016); the National Basic Research Program of China (2013CB632403); Jilin Province Science and Technology Development Projects (20150520003JH, 20140101041JC, 20130204001GX).

Appendix A. Supplementary data

Supplementary data associated with this article can be found, in the online version, at http://dx.doi.org/10.1016/j.snb.2015.10.063.

References

[1] G.J. Mohr, C. Demuth, U.E. Spichiger-Keller, Application of chromogenic and fluorogenic reactants in the optical sensing of dissolved aliphatic amines, Anal. Chem. 70 (1998) 3868–3873.
[2] D. Ju, H. Xu, Z. Qiu, J. Guo, J. Zhang, B. Cao, Highly sensitive and selective triethylamine-sensing properties of nanosheets directly grown on ceramic tube by forming NiO/ZnO PN heterojunction, Sens. Actuators B: Chem. 200 (2014) 288–296.
[3] T. Hernández-Jover, M. Izquierdo-Pulido, M.T. Veciana-Nogués, A. Mariné-Font, M.C. Vidal-Carou, Biogenic amine and polyamine contents in meat and meat products, J. Agric. Food Chem. 45 (1997) 2098–2102.
[4] B. Lee, R. Scopelliti, K. Severin, A molecular probe for the optical detection of biogenic amines, Chem. Commun. 47 (2011) 9639–9641.
[5] H. Karimi-Maleh, P. Biparva, M. Hatami, A novel modified carbon paste electrode based on NiO/CNTs nanocomposite and (9,10-dihydro-9,10-ethanoanthracene-11,12-dicarboximido)-4-ethylbenzene-1,2-diol as a mediator for simultaneous determination of cysteamine, nicotinamide adenine dinucleotide and folic acid, Biosens. Bioelectron. 48 (2013) 270–275.
[6] M. Najafi, M.A. Khalilzadeh, H. Karimi-Maleh, A new strategy for determination of bisphenol A in the presence of Sudan I using a ZnO/CNTs/ionic liquid paste electrode in food samples, Food Chem. 158 (2014) 125–131.
[7] H. Nohta, H. Satozono, K. Koiso, H. Yoshida, J. Ishida, M. Yamaguchi, Highly selective fluorometric determination of polyamines based on intramolecular excimer-forming derivatization with a pyrene-labeling reagent, Anal. Chem. 72 (2000) 4199–4204.
[8] S. Körsten, G.J. Mohr, Star-shaped tripodal chemosensors for the detection of aliphatic amines, Chem. Eur. J. 17 (2011) 969–975.
[9] W. Qin, P. Parzuchowski, W. Zhang, M.E. Meyerhoff, Optical sensor for amine vapors based on dimer-monomer equilibrium of indium(III) octaethylporphyrin in a polymeric film, Anal. Chem. 75 (2003) 332–340.
[10] W. Liu, M. Pink, D. Lee, Conjugated polymer sensors built on π-extended borasiloxane cages, J. Am. Chem. Soc. 131 (2009) 8703–8707.
[11] Y. Che, L. Zang, Enhanced fluorescence sensing of amine vapor based on ultrathin nanofibers, Chem. Commun. (2009) 5106–5108.
[12] X. Liu, X. Zhang, R. Lu, P. Xue, D. Xu, H. Zhou, Low-dimensional nanostructures fabricated from bis(dioxaborine)carbazole derivatives as fluorescent chemosensors for detecting organic amine vapors, J. Mater. Chem. 21 (2011) 8756–8765.
[13] A. Mallick, B. Garai, M.A. Addicoat, P.S. Petkov, T. Heine, R. Banerjee, Solid state organic amine detection in a photochromic porous metal organic framework, Chem. Sci. 6 (2015) 1420–1425.
[14] H. Xia, T. Liu, L. Gao, L. Yan, J. Wu, Development of film sensors based on ZnO nanoparticles for amine gas detection, Appl. Surf. Sci. 258 (2011) 254–259.
[15] M. Tong, G. Dai, D. Gao, WO_3 thin film sensor prepared by sol–gel technique and its low-temperature sensing properties to trimethylamine, Mater. Chem. Phys. 69 (2001) 176–179.
[16] X. Chu, S. Liang, W. Sun, W. Zhang, T. Chen, Q. Zhang, Trimethylamine sensing properties of sensors based on MoO_3 microrods, Sens. Actuators B: Chem. 148 (2010) 399–403.
[17] Y.H. Cho, Y.N. Ko, Y.C. Kang, I.D. Kim, J.H. Lee, Ultraselective and ultrasensitive detection of trimethylamine using MoO_3 nanoplates prepared by ultrasonic spray pyrolysis, Sens. Actuators B: Chem. 195 (2014) 189–196.
[18] C. Zamani, O. Casals, T. Andreu, J.R. Morante, A. Romano-Rodriguez, Detection of amines with chromium-doped WO_3 mesoporous material, Sens. Actuators B: Chem. 140 (2009) 557–562.
[19] W.H. Zhang, W.D. Zhang, Fabrication of SnO_2–ZnO nanocomposite sensor for selective sensing of trimethylamine and the freshness of fishes, Sens. Actuators B: Chem. 134 (2008) 403–408.
[20] H.S. Woo, C.W. Na, I.D. Kim, J.H. Lee, Highly sensitive and selective trimethylamine sensor using one-dimensional ZnO–Cr_2O_3 hetero-nanostructures, Nanotechnology 23 (2012) 245501–245511.
[21] C.H. Kwak, H.S. Woo, J.H. Lee, Selective trimethylamine sensors using Cr_2O_3-decorated SnO_2 nanowires, Sens. Actuators B: Chem. 204 (2014) 231–238.
[22] R.S. Niranjan, M.S. Londhe, A.B. Mandale, S.R. Sainkar, L.S. Prabhumirashi, K. Vijayamohanan, I.S. Mulla, Trimethylamine sensing properties of thorium-incorporated tin oxide, Sens. Actuators B: Chem. 87 (2002) 406–413.
[23] T. Guo, Y. Luo, Y. Zhang, Y.H. Lin, C.W. Nan, ZnO–NiO hetero-nanostructures as highly sensitive and selective triethylamine sensor, J. Appl. Phys. 116 (2014) 044309.
[24] Y. Che, X. Yang, Z. Zhang, J. Zuo, J.S. Moore, L. Zang, Ambient photodoping of p-type organic nanofibers: highly efficient photoswitching and electrical vapor sensing of amines, Chem. Commun. 46 (2010) 4127–4129.
[25] H. Liu, S. Chen, G. Wang, S.Z. Qiao, Ordered mesoporous core/shell SnO_2/C nanocomposite as high-capacity anode material for lithium-ion batteries, Chem. Eur. J. 19 (2013) 16897–16901.
[26] H. Kim, J. Cho, Hard templating synthesis of mesoporous and nanowire SnO_2 lithium battery anode materials, J. Mater. Chem. 18 (2008) 771–775.
[27] X. Wang, Z. Li, Q. Li, C. Wang, A. Chen, Z. Zhang, R. Fan, L. Yin, Ordered mesoporous SnO_2 with a highly crystalline state as anode material for lithium ion batteries with enhanced electrochemical performance, CrystEngComm 15 (2013) 3696–3704.
[28] T. Waitz, B. Becker, T. Wagner, T. Sauerwald, C.-D. Kohl, M. Tiemann, Ordered nanoporous SnO_2 gas sensors with high thermal stability, Sens. Actuators B: Chem. 150 (2010) 788–793.
[29] P. Gurunathan, P.M. Ette, K. Ramesha, Synthesis of hierarchically porous SnO_2 microspheres and performance evaluation as Li-ion battery anode by using different binders, ACS Appl. Mater. Interfaces 6 (2014) 16556–16564.
[30] G. Collins, M. Blömker, M. Osiak, J.D. Holmes, M. Bredol, C. O'Dwyer, Three-dimensionally ordered hierarchically porous tin dioxide inverse opals and immobilization of palladium nanoparticles for catalytic applications, Chem. Mater. 25 (2013) 4312–4320.
[31] X. Wang, S. Qiu, J. Liu, C. He, G. Lu, W. Liu, Synthesis of mesoporous SnO_2 spheres and application in gas sensors, Eur. J. Inorg. Chem. (2014) 863–869.
[32] Y. Chen, J. Ma, L. Yu, Q. Li, T. Wang, Mesoporous SnO_2 nanospheres formed via a water-evaporating process with superior electrochemical properties, CrystEngComm 14 (2012) 6170–6172.
[33] D. Chandra, N. Mukherjee, A. Mondal, A. Bhaumik, Design and synthesis of nanostructured porous SnO_2 with high surface areas and their optical and dielectric properties, J. Phys. Chem. C 112 (2008) 8668–8674.
[34] K. Shiva, S. Asokan, A.J. Bhattacharyya, Improved lithium cyclability and storage in a multi-sized pore (differential spacers) mesoporous SnO_2, Nanoscale 3 (2011) 1501–1503.
[35] P.P. Jin, X. Zou, L.J. Zhou, J. Zhao, H. Chen, Y. Tian, G.D. Li, Biopolymer-assisted construction of porous SnO_2 microspheres with enhanced sensing properties, Sens. Actuators B: Chem. 204 (2014) 142–148.
[36] L. Li, S. Chen, L. Xu, Y. Bai, Z. Nie, H. Liu, L. Qi, Template-free synthesis of uniform mesoporous SnO_2 nanospheres for efficient phosphopeptide enrichment, J. Mater. Chem. B 2 (2014) 1121–1124.
[37] S.C. Yeow, W.L. Ong, A.S.W. Wong, G.W. Ho, Template-free synthesis and gas sensing properties of well-controlled porous tin oxide nanospheres, Sens. Actuators B: Chem. 143 (2009) 295–301.
[38] H. Zhang, Q. He, X. Zhu, D. Pan, X. Deng, Z. Jiao, Surfactant-free solution phase synthesis of monodispersed SnO_2 hierarchical naostructures and gas sensing properties, CrystEngComm 14 (2012) 3169–3176.
[39] Z. Li, Q. Zhao, W. Fan, J. Zhan, Porous SnO_2 nanospheres as sensitive gas sensors for volatile organic compounds detection, Nanoscale 3 (2011) 1646–1652.
[40] S. Liu, G. Huang, J. Yu, T.W. Ng, H.Y. Yi, P.K. Wong, Porous fluorinated SnO_2 hollow nanospheres: transformative self-assembly and photocatalytic inactivation of bacteria, ACS Appl. Mater. Interfaces 6 (2014) 2407–2414.
[41] K.S.W. Sing, D.H. Everett, R.A.W. Haul, L. Moscou, R.A. Pierotti, J. Rouquerol, T. Siemieniewska, Reporting physisorption data for gas/solid systems with

special reference to the determination of surface area and porosity, Pure Appl. Chem. 57 (1985) 603–619.
[42] E. Mamontov, L. Vlcek, D.J. Wesolowski, P.T. Cumings, W. Wang, L.M. Anovitz, J. Rosenqvist, C.M. Brown, V.G. Sakai, Dynamics and structure of hydration water on rutile and cassiterite nanopowders studied by quasielastic neutron scattering and molecular dynamics simulations, J. Phys. Chem. C 111 (2007) 4328–4341.
[43] H.W. Wang, D.J. Wesolowski, T.E. Proffen, L. Vlcek, W. Wang, L.F. Allard, A.I. Kolesnikov, M. Feygenson, L.M. Anovitz, R.L. Paul, Structure and stability of SnO_2 nanocrystals and surface-bound water species, J. Am. Chem. Soc. 135 (2013) 6885–6895.
[44] P. Manjula, R. Boppella, S.V. Manorama, A facile and green approach for the controlled synthesis of porous SnO_2 nanospheres: application as an efficient photocatalyst and an excellent gas sensing material, ACS Appl. Mater. Interfaces 4 (2012) 6252–6260.
[45] C. Gadois, J. Swiatowska, S. Zanna, P. Marcus, Influence of titanium surface treatment on adsorption of primary amines, J. Phys. Chem. C 117 (2013) 1297–1307.
[46] J.L. Lin, Y.C. Lin, B.C. Lin, P.C. Lai, T.E. Chien, S.H. Li, Y.F. Lin, Adsorption and reactions on TiO_2: comparison of N,N-dimethylformamide and dimethylamine, J. Phys. Chem. C 118 (2014) 20291–20297.
[47] Y. Cao, X. Huang, Y. Wu, Y.-C. Zou, J. Zhao, G.-D. Li, X. Zou, Three-dimensional ultrathin In_2O_3 nanosheets with morphology-enhanced activity for amine sensing, RSC Adv. 5 (2015) 60541–60548.
[48] K. Suematsu, M. Yuasa, T. Kida, N. Yamazoe, K. Shimanoe, Effects of crystallite size and donor density on the sensor response of SnO_2 nano-particles in the state of volume depletion, J. Electrochem. Soc. 159 (2012) J136–J141.
[49] T. Kida, S. Fujiyama, K. Suematsu, M. Yuasa, K. Shimanoe, Pore and particle size control of gas sensing films using SnO_2 nanoparticles synthesized by seed-mediated growth: design of highly sensitive gas sensors, J. Phys. Chem. C 117 (2013) 17574–17582.
[50] T. Wagner, S. Haffer, C. Weinberger, D. Klaus, M. Tiemann, Mesoporous materials as gas sensors, Chem. Soc. Rev. 42 (2013) 4036–4053.
[51] G. Sakai, N. Matsunaga, K. Shimanoe, N. Yamazoe, Theory of gas-diffusion controlled sensitivity for thin film semiconductor gas sensor, Sens. Actuators B: Chem. 80 (2011) 125–131.

Biographies

Pan-Pan Jin is a master student in State Key Laboratory of Inorganic Synthesis & Preparative Chemistry, Jilin University in China. Her research interest is the synthesis of sensing nanomaterials.

Xiaoxi Huang received his B.S. degree from Peking University, Health Science Center, China, in 2011. He is currently a Ph.D. candidate in Department of Chemistry and Chemical Biology in Rutgers, the State University of New Jersey.

Yong-Cun Zou is a postdoctoral scholar in College of Electronic Science & Engineering, Jilin University in China. He received his Ph.D. from Jilin University (China) in 06/2014.

Li-Jing Zhou received her B.Sc. chemistry degree from Heibei North University, China, in 2009. Presently, she is a Ph.D. student at State Key Laboratory of Inorganic Synthesis & Preparative Chemistry, Jilin University in China.

Xue Wang is a master student in State Key Laboratory of Inorganic Synthesis & Preparative Chemistry, Jilin University in China. She has majored in the synthesis of hollow nanomaterials.

Feng Zhang is a lecturer at Dalian Polytechnic University. He obtained his Ph.D. in 2009 from Jilin University and worked as a postdoctoral research fellow in Changchun Institute of Applied Chemistry Chinese Academy of Sciences from 2009 to 2011. From 2011 to 2013, he worked in Dalian Institute of Chemical Physics Chinese Academy of Sciences. His current scientific interests are focused on the nanostructured materials for advanced energy conversion and storage devices.

De-Jun Wang is a full professor of physical chemistry at College of Chemistry, Jilin University in China. He received his B.Sc. (1977), M.Sc. (1983) and Ph.D. (1989) from Jilin University. His interests include photoelectric sensors, photocatalysts and related materials.

Guo-Dong Li is a full professor at State Key Lab of Inorganic Synthesis & Preparative Chemistry, College of Chemistry, Jilin University in China. He received his B.Sc. (1995), M.Sc. (1998) and Ph.D. (2001) from Jilin University. His research interests include chemical sensors, lithium batteries, photocatalysts.